



# Optics Letters

## Subwavelength structure engineered passband filter for the 2- $\mu\text{m}$ wave band

WENCHANG HE,<sup>1,†</sup> YUHAN SUN,<sup>1,†</sup> PEIJI ZHOU,<sup>1,†</sup> LIPENG XIA,<sup>1</sup> TING LI,<sup>1</sup> QIYUAN YI,<sup>2</sup> LI SHEN,<sup>2,4</sup>  ZHENZHOU CHENG,<sup>3,5</sup>  AND YI ZOU<sup>1,\*</sup> 

<sup>1</sup>School of Information Science and Technology, ShanghaiTech University, Shanghai 201210, China

<sup>2</sup>Wuhan National Laboratory for Optoelectronics, School of Optical and Electronic Information, Huazhong University of Science and Technology, Wuhan 430074, China

<sup>3</sup>School of Precision Instruments and Optoelectronics Engineering, Tianjin University, Tianjin 300072, China

<sup>4</sup>e-mail: lishen@hust.edu.cn

<sup>5</sup>e-mail: zhenzhoucheng@tju.edu.cn

\*Corresponding author: zouyi@shanghaitech.edu.cn

†These authors contributed equally to this Letter.

Received 21 November 2022; revised 27 December 2022; accepted 27 December 2022; posted 3 January 2023; published 31 January 2023

**In this work, we experimentally demonstrate a passband filter for the 2- $\mu\text{m}$  wave band on the silicon-on-insulator platform. The device consists of a strip waveguide and an apodized subwavelength-structured waveguide. Fabricated on a 340-nm-thick silicon membrane, the proposed passband filter shows a 3-dB bandwidth of 16–33 nm, a high sidelobe suppression ratio (SLSR) of 24 dB, and a low insertion loss (IL) of 0.4 dB.** © 2023 Optica Publishing Group

<https://doi.org/10.1364/OL.481426>

In recent years, due to the emergence of ultralow latency, low-loss hollow-core fiber (HCF) [1], and high-gain, low-noise thulium-doped fiber amplifiers [2], the 2- $\mu\text{m}$  wave band has attracted lots of attention, especially for optical communication systems which require a large capacity and low latency [3]. Conventional silicon-on-insulator (SOI) is the preferred platform for 2- $\mu\text{m}$  wave-band integrated devices due to its low material loss, high integration density, and complementary metal-oxide semiconductor (CMOS) compatibility [4]. However, since the optical mode size in the 2- $\mu\text{m}$  wave band is larger than the telecommunication wave band, optical waveguides of the commonly used SOI chip with a 220-nm-thick top silicon layer become less confined [5]. Therefore, an SOI with a thicker silicon layer, e.g., 340 nm, usually possesses better performance at the 2- $\mu\text{m}$  wave band.

For an SOI with 2- $\mu\text{m}$ -thick buried oxide, our simulation shows that, compared with the 220-nm SOI, the 340-nm SOI reduces the leakage optical intensity by 8.3 dB and 26.6 dB for the transverse electric (TE) and transverse magnetic (TM) slab modes, respectively. Such an effect may improve device performance in the 2- $\mu\text{m}$  wave band. For example, as shown in Table 1, the coupling efficiency of a shallow-etched one-dimensional grating coupler (GC) based on a 340-nm-thick silicon layer is higher than that of a 220-nm-thick silicon layer. Besides, for microring resonators (MRRs), the Q factor of the 340-nm silicon device is higher because of better mode confinement, while, for a similar reason, the multimode interferometer (MMI)

splitter presents a lower insertion loss on 340-nm-thick silicon. More recently, a simulation predicted that 340-nm-thick SOI-based Mach-Zehnder modulators (MZM) exhibit lower loss and higher modulation efficiency in the 2- $\mu\text{m}$  wave band than those with a 220-nm silicon layer. So far, several photonic devices at the 2- $\mu\text{m}$  wave band that are based on the SOI platform with 340-nm-thick top silicon have been demonstrated, such as GCs [6], MRRs [6,7], MMI splitters [8,9], MZMs [5], and subwavelength grating slot waveguides (SSWs) [10].

Optical passband filters are one of the most important devices for integrated photonic systems [12–15]. Passband filters in the 2- $\mu\text{m}$  wave band have also been proposed, e.g., an MRR-based narrowband filter [4] and a Bragg-grating-based broadband filter [16]. In particular, Ref. [16] demonstrated a passband filter with a high sidelobe suppression ratio (SLSR) and a low insertion loss by using a multimode waveguide grating and a pair of two-channel mode (de)multiplexers. Such a filter is very useful in telecommunication and sensing. However, both devices are on a 220-nm-thick SOI. To the best of our knowledge, 2- $\mu\text{m}$  wave band passband filters have been seldom reported on the SOI platform with a 340-nm-thick top silicon layer. Moreover, other filters, such as directional coupler (DC)-based filters, are also desired to enrich the filtering technologies in the 2- $\mu\text{m}$  wave band.

In this work, we experimentally demonstrate a passband filter operating in the 2- $\mu\text{m}$  wave band on a 340-nm SOI. The proposed filter consists of a strip waveguide and an apodized subwavelength-structured waveguide (SSW) to form an asymmetric directional coupler. By engineering the structural parameters of the strip waveguide and the SSW, the respective fundamental mode of the two waveguides meets the phase-matching condition at the center wavelength. Moreover, the sidelobes are effectively suppressed through apodization by varying the separation of the two waveguides as a function of position along the propagation direction. For the passband filter demonstrated here, the measured spectra exhibit a 3-dB bandwidth (BW) of 16–33 nm, a high sidelobe suppression ratio (SLSR) of 24 dB, and a low insertion loss (IL) of 0.4 dB. Table 2

**Table 1. Performance Comparison of Devices on 220-nm/340-nm-Thick Silicon in the 2- $\mu$ m Wave Band**

Device/ Performance	220 nm SOI	340 nm SOI	Simu. or Exp. <sup>a</sup>
GC/Coupling	-8.4 dB [4],	-6.5 dB [6]	Exp.
Efficiency	-7.9 dB [11]		
MRR/Q	1520 [4]	11200 [6]	Exp.
Factor			
MMI Splitter/ Insertion Loss	3.03±0.43 dB [11]	0.29±0.01 dB [9]	Exp.
MZM/Loss	7.07 dB/cm@4 V [5]	5.17 dB/cm@4 V [5]	Sim.
MZM/ Modulation Efficiency	3.17 V·cm @4 V [5]	2.86 V·cm @4 V [5]	Sim.

<sup>a</sup>“Sim.” and “Exp.” represent “simulation result” and “experimental result,” respectively.

**Table 2. Performance Comparison of Passband Filters in the 2- $\mu$ m Wave Band**

Ref.	Si Layer Thickness (nm)	SLSR (dB)	IL (dB)	BW (nm)
[4]	220	>20 <sup>a</sup>	~2.5	~2 (3 dB)
[16]	220	>20	1	6–26 (0.5 dB)
This Work	340	24	<0.5	16–33 (3 dB)

<sup>a</sup>In Ref. [4], this is the extinction ratio rather than the SLSR.

shows a performance comparison of passband filters in the 2- $\mu$ m wave band. Our device exhibits a higher measured SLSR and a lower IL. Such a filter may find important applications in sensing [17], spectral filtering [18], dispersion engineering [19,20], and so on.

Figures 1(a) and 1(b) show a three-dimensional (3D) schematic and the top view of the proposed passband filter, respectively. The inset in Fig. 1(a) is a zoomed-in view of the SSW taper at the cross port. The device is composed of two waveguides, i.e., a strip waveguide and an apodized SSW. Compared with a conventional strip waveguide, SSWs provide additional design freedom for waveguide engineering [21] and achieve the phase-matching condition even with different waveguide widths. Due to different mode effective index changing rates of the strip waveguide and the SSW, they meet the phase-matching condition only at a specific wavelength:

$$n_{eff1}(\lambda) = n_{eff2}(\lambda). \quad (1)$$

Here,  $n_{eff1}$  and  $n_{eff2}$  are the effective indices of the fundamental mode of the strip waveguide and the Bloch mode of the SSW waveguide, respectively. We first simulate the property of the SSW. To be fabrication friendly, we set its period to 300 nm and the duty cycle to 0.5. Then we calculate the band diagram of SSWs with different widths using the finite element method (FEM) [22] and plot it in Fig. 1(c), from which we get  $n_{eff2}$  as

$$n_{eff2} = c \frac{K_z(\omega)}{\omega}. \quad (2)$$

Here,  $K_z$  is the Bloch wavenumber along the propagation direction and  $c$  is the speed of light in a vacuum.

Designing a filter with its center wavelength at around 2  $\mu$ m requires the fulfillment of Eq. (1) when  $\lambda \approx 2\mu$ m. Therefore,

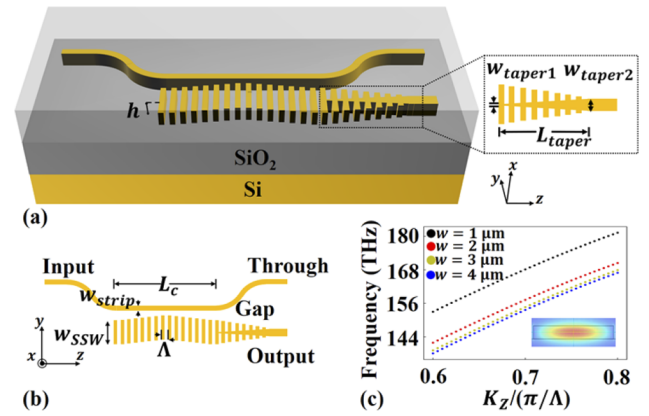


**Fig. 1.** (a) Schematic 3D and (b) top views of the proposed SOI filter. Here,  $w_{strip} = 0.48 \mu\text{m}$ ,  $w_{SSW} = 3.7 \mu\text{m}$ ,  $h = 340 \text{ nm}$ , and  $\Lambda = 300 \text{ nm}$ . The inset in (a) is the top view of the SSW taper. Here,  $w_{taper1} = 100 \text{ nm}$ ,  $w_{taper2} = 600 \text{ nm}$ , and  $L_{taper} = 15 \mu\text{m}$ . (c) Band diagram of SSWs with different widths.

we scan the effective index values of strip waveguides with different widths from 0.45  $\mu\text{m}$  to 0.5  $\mu\text{m}$  with a step of 0.1  $\mu\text{m}$  using the finite difference eigenmode (FDE) method. Considering the material dispersion, we plot  $n_{eff1}$  and  $n_{eff2}$  as a function of wavelength for different waveguide widths in Fig. 2(a). As shown in Fig. 2(a), when scanning the width of the SSW from 3  $\mu\text{m}$  to 4  $\mu\text{m}$  with a step of 0.1  $\mu\text{m}$ , there are multiple intersections in the wavelength range from 1.95  $\mu\text{m}$  to 2.05  $\mu\text{m}$ , indicating the existence of phase matching at these specific wavelengths. However, considering our light source centered at 2.02  $\mu\text{m}$ , we choose  $w_{strip} = 0.48 \mu\text{m}$  and  $w_{SSW} = 3.7 \mu\text{m}$  for our filter design, as circled and shown in the inset of Fig. 2(a), to achieve complete light coupling at 2.02  $\mu\text{m}$ . In addition, we also simulate the SSW taper with the 3D finite difference time domain (FDTD) method. As shown in the inset of Fig. 1(a), we keep the period and duty cycle of the taper the same as for the SSW and set  $w_{taper1} = 100 \text{ nm}$ ,  $w_{taper2} = 600 \text{ nm}$ , and  $L_{taper} = 15 \mu\text{m}$ . Figure 2(b) shows the simulated transmission and backreflection of the taper. High transmission ( $> -0.08 \text{ dB}$ ) and low backward reflection ( $< -17 \text{ dB}$ ) are exhibited for the region from 1.9 to 2.1  $\mu\text{m}$ , with  $-40 \text{ dB}$  backreflection at a wavelength of 2.02  $\mu\text{m}$ . The inset is the electric field of the taper at 2.02  $\mu\text{m}$ .

Moreover, in order to improve the SLSR, we apodize the SSW along the propagation direction by modulating the gap with a Gaussian function of the position  $z$  along the propagation direction [23]:

$$G(z) = G_{min} + R \left[ 1 - \exp \left( \frac{-a(z - 0.5L)^2}{L^2} \right) \right], \quad (3)$$

where  $G_{min}$  is the minimum gap and  $L$  is the length of the coupling region.  $a$  and  $R$  are parameters associated with apodization that represent the width and amplitude of the Gaussian curve, respectively. In this work, since the roles of  $a$  and  $R$  are similar, we fix  $R = 1 \mu\text{m}$  and optimize the other parameters jointly, i.e.,  $G_{min}$ ,  $a$ , and  $L$ , to achieve better performance of the device.

We simulate the devices using the 3D FDTD method and plot them in Fig. 3. Firstly, to ensure a low device insertion loss, we tune  $G_{min}$  to fit different  $a$  and  $L$ . As shown in Fig. 3(a), when  $a = 0$  and  $L = 200 \mu\text{m}$ , adjusting  $G_{min}$  from 0.3  $\mu\text{m}$  to 0.4  $\mu\text{m}$

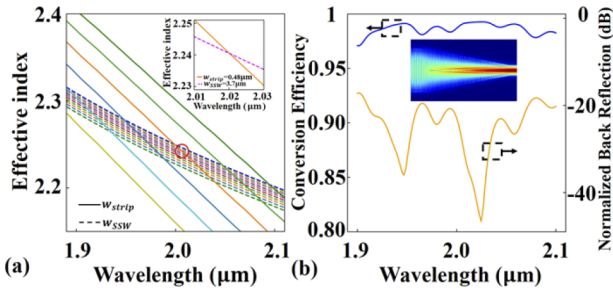


**Fig. 2.** (a) Effective index variations as a function of wavelength for strip waveguides (solid line) and SSWs (dashed line) with different waveguide widths. Here, the  $w_{strip}$  is scanned from 0.45  $\mu\text{m}$  to 0.5  $\mu\text{m}$  with a step of 0.1  $\mu\text{m}$ , and the  $w_{SSW}$  is scanned from 3  $\mu\text{m}$  to 4  $\mu\text{m}$  with a step of 0.1  $\mu\text{m}$ . (b) Simulated transmission and backreflection spectra for the SSW taper. The inset displays the electric field for the taper at 2.02  $\mu\text{m}$  wavelength.

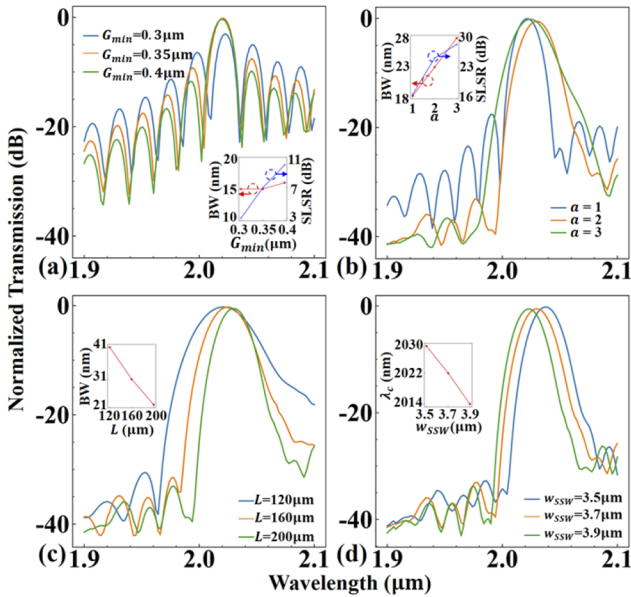


**Fig. 3.** Simulated output spectra of the filters with (a) different  $G_{min}$  values when  $L = 200 \mu\text{m}$  and  $a = 0$  (the inset is a plot of BW and SLSR versus  $G_{min}$ ), (b) different  $a$  values when  $L = 200 \mu\text{m}$  and  $G_{min}$  is within the range of 0.25  $\mu\text{m}$  to 0.35  $\mu\text{m}$  (the inset is a plot of BW and SLSR versus  $a$ ), (c) different  $L$  values when  $a = 2$  and  $G_{min}$  is within the range of 0.2  $\mu\text{m}$  to 0.3  $\mu\text{m}$  (the inset is a plot of BW versus  $L$ ), and (d) different  $w_{SSW}$  values when  $a = 2$  and  $G_{min} = 0.3 \mu\text{m}$  (the inset is a plot of the center wavelength  $\lambda_c$  versus  $w_{SSW}$ ).

could reduce the insertion loss at the center wavelength. Meanwhile, the SLSR increases for a bigger  $G_{min}$ , while the BW and the center wavelength barely change. Moreover, since a larger SLSR can be obtained by increasing the apodization strength  $a$ , we increase  $a$  from 1 to 3 in Fig. 3(b). The SLSR exhibits a significant improvement from 17 dB to 28 dB. However, the BW also expands from 19 nm to 27 nm. To achieve both a high SLSR and an appropriate BW, we set  $a = 2$  for our device, which shows a BW of 23 nm and an SLSR of 25 dB. Note that during the simulation for Figs. 3(b)–3(d), we adjust the  $G_{min}$  to guarantee a low insertion loss. Besides, we also explore the effects of device parameters on BW and the center wavelength. For the BW tuning, besides changing the apodization strength  $a$ , which

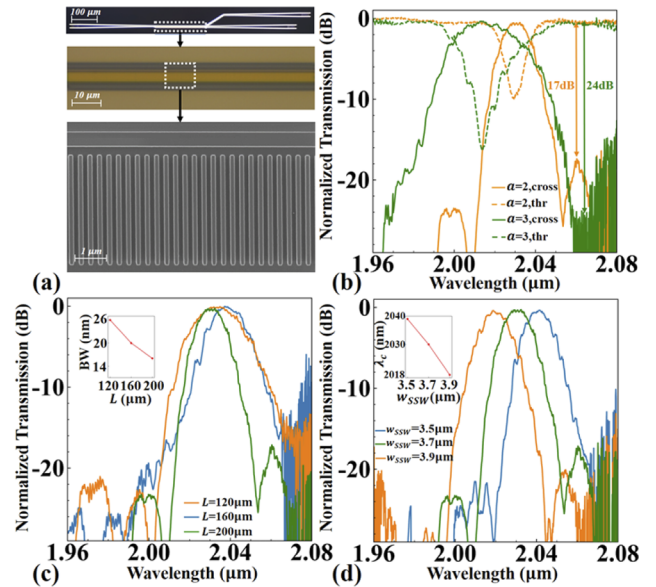


**Fig. 4.** (a) Microscope images of the entire device and the coupling region, and SEM photo of the strip and SSW waveguides. (b) Measured spectra at the cross port and through port of the filters with  $a = 2$  and 3 when  $L = 200 \mu\text{m}$ , respectively, for achieving negligible insertion loss. (c) Measured spectra of the filters with  $L$  from 120  $\mu\text{m}$  to 200  $\mu\text{m}$  when  $a = 2$  and  $G_{min}$  ranges from 0.2  $\mu\text{m}$  to 0.3  $\mu\text{m}$ . The inset is a plot of BW versus  $L$ . (d) Measured spectra of the filters with  $w_{SSW}$  ranging from 3.5  $\mu\text{m}$  to 3.9  $\mu\text{m}$  when  $a = 2$  and  $G_{min} = 0.3 \mu\text{m}$ . The inset is a plot of  $\lambda_c$  versus  $w_{SSW}$ .

also affects the SLSR, a more effective way is to modify the coupling length  $L$ . As shown in Fig. 3(c), upon increasing  $L$ , the BW narrows from 41 nm to 23 nm. In addition, as pointed out in Fig. 2(a), the center wavelength  $\lambda_c$  of the device can be shifted by changing the width of the SSW. Figure 3(d) shows the center wavelength shifting from 2014 nm to 2029 nm as we narrow the  $w_{SSW}$  from 3.9  $\mu\text{m}$  to 3.5  $\mu\text{m}$ .

The devices are fabricated in the ShanghaiTech University Quantum Device Lab. Figure 4(a) shows microscope images of the entire device and the zoomed-in coupling region, and a scanning electron microscope (SEM) picture of the strip and SSW waveguides. The device is fabricated on an SOI chip with a 340-nm-thick top silicon layer and a 2- $\mu\text{m}$ -thick buried dioxide layer with a similar process as described in Ref. [24]. The designed layout is defined by electron-beam lithography (EBL) on the ZEP-520A resist. Then the pattern is transferred to the silicon layer using induced coupled plasma (ICP). Finally, a 2- $\mu\text{m}$ -thick silicon dioxide layer is deposited over the entire device as a top cladding by plasma-enhanced chemical vapor deposition (PECVD).

In the experiment, a broadband 2- $\mu\text{m}$  amplified spontaneous emission (ASE) source is polarized and transmitted through a polarization-maintaining (PM) fiber. The light is then grating coupled into the chip and passes through the designed filter. The output signal is collected by an optical spectrum analyzer (OSA). By normalizing the output spectra to a reference waveguide, which is a single-mode strip waveguide connected to grating couplers at both ends, we obtain the normalized transmission shown in Figs. 4(b)–4(d). Figure 4(b) shows the measured spectra at the cross and through ports of the devices with  $a = 2$  and

3 when  $L = 200 \text{ }\mu\text{m}$ . The device with  $a = 2$  possesses a BW of 16 nm and an SLSR of 17 dB with an ignorable IL of 0.4 dB at 2030 nm. By increasing the apodization strength  $a$  from 2 to 3, the device exhibits a significantly improved SLSR of 24 dB, a wider BW of 33 nm, and a negligible IL of 0.3 dB. Moreover, the spectra of the BW and the center wavelength are shown in Figs. 4(c) and 4(d), respectively. On the one hand, we could control the BW by tuning the  $L$  of the device. As shown in Fig. 4(c), the BW narrows from 26 nm to 16 nm when increasing  $L$ . On the other hand, for the center wavelength, Fig. 4(d) indicates that it shifts from 2018 nm to 2040 nm upon shrinking the  $w_{\text{SSW}}$ . Note that the significantly higher noise floor at longer wavelengths, as shown in both Figs. 4(c) and 4(d), is mainly due to the low output power, which is limited by our light source. We also observe ripples with a free spectral range (FSR) of  $\sim 4 \text{ nm}$  in the spectra, which corresponds to a cavity length comparable to our taper between the grating coupler and the single mode region. Further improving the taper design, e.g., using a longer linear taper, employing special curves, etc., may solve this issue. The experimental results are consistent with our simulation, but with slightly smaller SLSRs and a redshifted center wavelength, which may be caused by an imperfect fabrication process.

In summary, we have demonstrated a passband filter for the 2- $\mu\text{m}$  wave band on a 340-nm SOI platform. By engineering the strip-SSW-based asymmetric DC, a high SLSR ratio of 24 dB is experimentally obtained. Meanwhile, the fabricated filter also shows a BW of 16–33 nm and a negligible IL of less than 0.4 dB. The measurement results agree well with our simulation, proving the feasibility of our approach for building filters on the SOI platform.

**Funding.** National Natural Science Foundation of China (51874301, 61705099, 62175080); Natural Science Foundation of Shanghai (21ZR1443100); Science and Technology Commission of Shanghai Municipality (Y7360k1D01).

**Disclosures.** The authors declare no conflicts of interest.

**Data availability.** Data underlying the results presented in this paper are not publicly available at this time but may be obtained from the authors upon reasonable request.

## REFERENCES

1. W. Shen, J. Du, L. Sun, C. Wang, Y. Zhu, K. Xu, B. Chen, and Z. He, *J. Lightwave Technol.* **38**, 3874 (2020).

2. Z. Li, A. M. Heidt, J. M. Daniel, Y. Jung, S. U. Alam, and D. J. Richardson, *Opt. Express* **21**, 9289 (2013).
3. W. Shen, P. Zeng, Z. Yang, D. Xia, J. Du, B. Zhang, K. Xu, Z. He, and Z. Li, *Photonics Res.* **8**, 1484 (2020).
4. J. Li, Y. Liu, Y. Meng, K. Xu, J. Du, F. Wang, Z. He, and Q. Song, *IEEE Photonics Technol. Lett.* **30**, 471 (2018).
5. Y. Liu, X. Li, S. Wang, W. Yue, Y. Cai, and M. Yu, *Infrared Laser Eng.* **51**, 20220092 (2022).
6. Z. Zhang, G. I. Ng, H. Qiu, W. Wang, X. Guo, M. S. Rouified, C. Liu, and H. Wang, *Appl. Opt.* **56**, 5444 (2017).
7. Z. Zhang, J. Zhou, C. G. Littlejohns, G. T. Reed, H. Wang, G. I. Ng, T. Hu, H. Qiu, X. Guo, W. Wang, M. S. Rouified, C. Liu, and J. Sia, *IEEE Photonics J.* **10**, 1 (2018).
8. M. S. Rouified, C. G. Littlejohns, G. X. Tina, Q. Haodong, T. Hu, Z. Zhang, C. Liu, G. T. Reed, and H. Wang, *IEEE Photonics Technol. Lett.* **28**, 2827 (2016).
9. M. S. Rouified, C. G. Littlejohns, G. X. Tina, H. Qiu, J. S. Penades, M. Nedeljkovic, Z. Zhang, C. Liu, D. J. Thomson, G. Z. Mashanovich, G. T. Reed, and H. Wang, *Opt. Express* **25**, 10893 (2017).
10. Z. Ruan, L. Shen, S. Zheng, A. Wang, Y. Long, N. Zhou, and J. Wang, *Nanophotonics* **7**, 865 (2018).
11. H. Ma, H. Yang, B. Tang, M. Wei, J. Li, J. Wu, P. Zhang, C. Sun, L. Li, and H. Lin, *Chin. Opt. Lett.* **19**, 071301 (2021).
12. H. Yan, Y. Zou, S. Chakravarty, C. J. Yang, Z. Wang, N. Tang, D. Fan, and R. T. Chen, *Appl. Phys. Lett.* **106**, 121103 (2015).
13. B. Liu, Y. Zhang, Y. He, X. Jiang, J. Peng, C. Qiu, and Y. Su, *Opt. Express* **25**, 11359 (2017).
14. B. Naghdi and L. R. Chen, *Opt. Express* **24**, 23429 (2016).
15. D. Charron, J. St-Yves, O. Jafari, S. LaRochelle, and W. Shi, *Opt. Lett.* **43**, 895 (2018).
16. D. Liu, H. Wu, and D. Dai, *J. Lightwave Technol.* **37**, 2217 (2019).
17. Y. Zou, S. Chakravarty, L. Zhu, and R. T. Chen, *Appl. Phys. Lett.* **104**, 141103 (2014).
18. G. Zhan, R. Liang, H. Liang, J. Luo, and R. Zhao, *Opt. Express* **22**, 9912 (2014).
19. A. D. Simard and S. LaRochelle, *Opt. Express* **23**, 16662 (2015).
20. J. Huang, H. Han, A. Liu, H. Wang, X. Liu, Y. Zou, M. Lu, and Y. Chen, *IEEE Photonics J.* **9**, 1 (2017).
21. Y. Zou, H. Subbaraman, S. Chakravarty, X. Xu, A. Hosseini, W. C. Lai, P. Wray, and R. T. Chen, *Opt. Lett.* **39**, 3070 (2014).
22. A. Gervais, P. Jean, W. Shi, and S. LaRochelle, *IEEE J. Sel. Top. Quantum Electron.* **25**, 1 (2019).
23. W. Shi, X. Wang, C. Lin, H. Yun, Y. Liu, T. Baehr-Jones, M. Hochberg, N. A. F. Jaeger, and L. Chrostowski, *Opt. Express* **21**, 3633 (2013).
24. A. Zhang, L. Xia, T. Li, C. Chang, P. Zhou, X. Xu, and Y. Zou, *Opt. Lett.* **46**, 5000 (2021).